Catal Lett (2012) 142:480–485
DOI 10.1007/s10562-012-0768-6

Preparation and Characterization of Mesoporous MoO_3/TiO_2 Composite with High Surface Area by Self-Supporting and Ammonia Method

Licheng Li · Yanfang Wang · Kangzhong Shi · Shanshan Chen · Zhuhong Yang · Xiaohua Lu

Received: 28 November 2011 / Accepted: 6 January 2012 / Published online: 22 February 2012

Abstract A mesoporous MoO_3/TiO_2 composite was prepared from titanate derivative by consecutive self-supporting and ammonia method. All samples were characterized by X-ray Diffraction, N_2 adsorption–desorption, Raman Spectra and Field-Emission Scanning Electron Microscopy. The results showed that mesoporous MoO_3/TiO_2 composite had a higher surface area (173 m^2/g) and a better MoO_3 dispersion than that prepared by traditional impregnation (90 m^2/g). As for hydrodesulfurization tests, mesoporous MoO_3/TiO_2 composite in this case presented a better catalytic performance, attributed to its high surface area and good dispersion of MoO_3. It can be found that self-supporting played a key role in preparing mesoporous MoO_3/TiO_2 composite with high surface area. Additionally, aqueous ammonia could effectively dissolve excess MoO_3, which helped to obtain mesoporous MoO_3/TiO_2 composite with better dispersion of MoO_3.

Keywords Titanium oxide · Molybdenum oxide · Self-supporting · High surface area · Hydrodesulfurization

1 Introduction

MoO_3/TiO_2 composites have attracted much attention in many industrial reactions, such as hydrodesulfurization (HDS), selective reduction, and isomerization [1–5]. Due to the synergetic effect between TiO_2 and molybdenum species, MoO_3/TiO_2 composites present excellent catalytic performance compared with other molybdenum composites [2, 6, 7]. Furthermore, catalytic efficiency of composites also depends on their structure that is greatly influenced by the preparation process [8–10]. Generally, the composites with high surface area and mesoporous structure are considered to have better catalytic performance, especially in catalytic reactions of large molecules [11, 12]. However, TiO_2 usually has a lower surface area (<50 m^2/g) than other conventional support materials (such as SiO_2 and Al_2O_3) [13, 14]. This means that the amount of MoO_3 species on TiO_2 is severely limited. As a result, the activity of MoO_3/TiO_2 can't be improved much because of its poor textural properties.

To overcome this disadvantage, some efforts have been focused on to improve textural properties by various methods. For instance, good results have been obtained by sol–gel technique [15, 16], although this technique needs to be carried out under strict conditions. Another is template method [17–20], including soft template and hard template. By template method, amorphous materials with fine structure (high surface area or uniform pore size) are obtained at first, and then followed by removing the template to get crystallized porous materials. To date, mesoporous materials reported in literatures were generally prepared by template method. However, it should be noticed that the template residue may influence the materials' applications [20, 21].

In our previous work, we have prepared an amorphous porous titanate derivative (TiD) from potassium dititanate using a novel template-free method. Mesoporous titania with high surface area was acquired by thermal crystallization of titanate derivate [22, 23], where the corresponding supported MoO_3 composite showed high activity and

L. Li · Y. Wang · K. Shi · Z. Yang (✉) · X. Lu
State Key Laboratory of Materials-Oriented Chemical Engineering, Nanjing University of Technology, Nanjing 210009, China
e-mail: zhhyang@njut.edu.cn

S. Chen
State Key Laboratory of Catalysis, Dalian Institute of Chemical Physics, Chinese Academy of Sciences, Dalian 116023, China

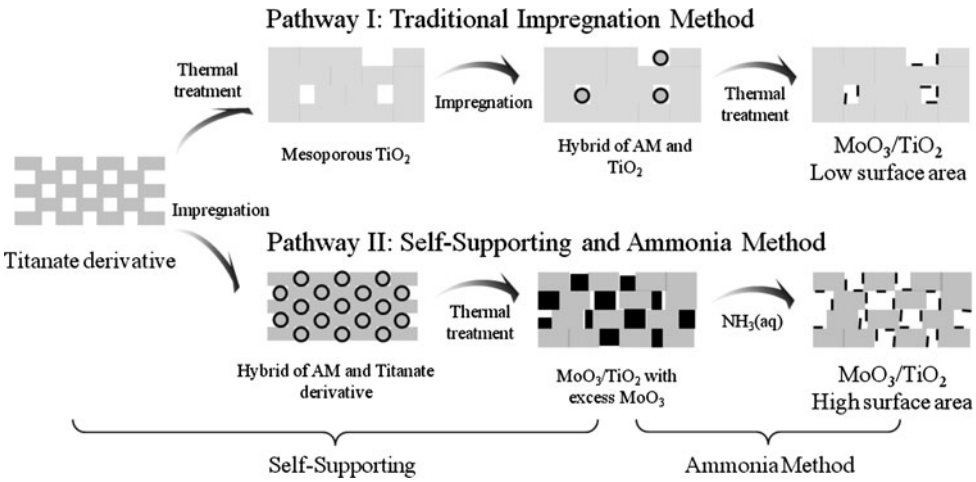

Fig. 1 Scheme for the preparation of mesoporous MoO_3/TiO_2 composite

stability in HDS [24, 25]. Inspired by hard template, the improved preparation of mesoporous MoO_3/TiO_2 composite was carried out by self-supporting and ammonia method described as follows (Fig. 1). Firstly, the inside of the pores of the amorphous TiD was filled with a large number of MoO_3 precursors, followed by thermal treatment for crystallization. During the thermal treatment, the pore structure of TiO_2 can be preserved by MoO_3. And then excess MoO_3 was dissolved and washed out by aqueous ammonia, while the insoluble MoO_3 species were strongly bound to TiO_2 and remained in the composite. The MoO_3 species could be used as a catalytic active component [7]. Thus, noteworthy is that this self-supporting of MoO_3/TiO_2 composite needn't be worried about the residual impurities, which is different from conventional template method. The mesoporous MoO_3/TiO_2 composite was characterized by various physical and chemical methods and its characteristics were compared with those of the composite prepared via traditional impregnation. The catalytic performance of composites was also evaluated in a HDS process using a fixed bed reactor.

2 Experimental Section

2.1 Materials

Ammonium molybdate tetrahydrate ($(NH_4)_6Mo_7O_{24}\bullet 4H_2O$, Sinopharm Chemical Reagent Co., Ltd), ammonia ($NH_3\cdot H_2O$, Nanjing Chemical Reagent Co., Ltd), dibenzothiophene (DBT) ($C_{12}H_8S$, Acros Organics), decalin ($C_{10}H_{18}$, Sinopharm Chemical Reagent Co., Ltd), carbon disulfide (CS_2, Sinopharm Chemical Reagent Co., Ltd), and deionized water were used as received. TiD and mesoporous TiO_2 were prepared according to our previous work [22, 23]. The structural data of these two materials were shown in Table 1.

Table 1 Textural characteristics and chemical compositions of various samples

Sample	Surface area (m^2/g)	Pore volume (cm^3/g)	Average pore size (nm)	MoO_3 Content (%)
TiD	257	0.17	–	–
TiO_2	103	0.20	6.4	–
$MoO_3(I)/TiO_2$	37	0.08	–	61
MoO_3/TiO_2	173	0.21	4.9	14
Control sample	90	0.17	5.9	12

2.2 Preparation of Composites

Mesoporous MoO_3/TiO_2 composite was prepared in two main steps. Firstly, 10.0 g of $(NH_4)_6Mo_7O_{24}\cdot 4H_2O$ (AM) was dissolved in 35 mL of deionized water with stirring, then 5.0 g of the dried TiD powers was added. After stirring for 0.5 h, the excess water was evaporated by heating with continuous stirring. The mixture was dried at 100 °C and calcined at 500 °C for 2 h. MoO_3/TiO_2 composite with excess MoO_3 was an intermediate, which was designated as $MoO_3(I)/TiO_2$. Secondly, the excess MoO_3 was then removed by ammonia method. $MoO_3(I)/TiO_2$ was immersed into the ammonia (>50 mL ammonia/g $MoO_3(I)/TiO_2$) with stirring for 6 h and centrifugal separating. The collected precipitate was suspended in ammonia again with stirring, and the process was repeated for four times to sufficiently dissolve the excess MoO_3. Then the resulting gray powder was washed by deionized water, dried in the air to obtain the final mesoporous MoO_3/TiO_2 composite.

For comparison, a control sample was prepared by traditional impregnation method. Mesoporous TiO_2 obtained by calcinations of TiD at 500 °C for 2 h was impregnated with an $(NH_4)_6Mo_7O_{24}\cdot 4H_2O$ aqueous solution, followed by calcinations at 500 °C for 2 h. MoO_3 content of control sample was set at 12 wt% according to the dispersion thresholds of TiO_2 [13, 26].

2.3 Characterizations

X-ray diffraction (XRD) analysis of samples was carried out on a D8 Adavance X-ray diffractometer using Cu Kα radiation under the setting conditions of 40 kV and 30 mA. The scan ranged from 5° to 60° at a rate of 0.2 s/step. Structural properties of samples were determined by N_2 adsorption–desorption (at −196 °C) in a Micromeritics Tristar II 3020M apparatus. Surface areas were calculated by BET method (S_{BET}), pore volume (V_P) was determined by nitrogen adsorption at a relative pressure of 0.99. Pore size distributions were found from adsorption isotherms by BJH method. The composition of samples was obtained on an Optima 2000 DV ICP-OES instrument. Hitachi S-4800 field-emission scanning electron microscopy (FESEM) was used to characterize the micro-morphology of samples with operating voltage of 5 kV. Raman Spectra were obtained using a Horiba HR 800 spectrometer, equipped with a CCD camera detector. As a source of excitation the 514 nm line of a Spectra Physics 2018 Argon/Krypton Ion Laser system were focused through an Olympus BX41 microscope equipped with a 50 magnification objective. The laser power never exceeded 5 mW for each sample.

2.4 Catalytic Activity Test

Catalytic hydrodesulphurization performances of the composites were conducted in a high-pressure micro-fix-bed continuous-flow reactor with 0.333 g of composites (20–40 U.S. standard mesh size particles diluted with ca. 1 mL of quartz sands). Ahead of HDS reaction, composites were in situ sulfided for 8 h with a 3% CS_2/decalin mixture under the conditions of 300 °C, 2 MPa, LHSV 6 h^{-1} and H_2 to mixture volumetric ratio 600. After sulphurization process, the inlet feedstock was switched to a 1 wt% DBT/decalin mixture and the operation conditions were consistent to the sulphurization process. After 6 h of on-stream reaction, liquid products were collected and analyzed in an SP-6890 gas chromatograph. The HDS efficiencies of appointed composites were determined by the conversion of DBT.

3 Results and Discussion

3.1 N_2 Adsorption–Desorption, XRD, and FESEM Analyses

The detailed structural parameters of various materials, such as BET specific area, pore volume, and average pore size, are listed in Table 1. BET specific area is 173 m^2/g for mesoporous MoO_3/TiO_2 composite prepared by improved preparation in this paper. However, as for the composite prepared through traditional impregnation pathway, BET specific area is 90 m^2/g, which is still larger than that of conventional TiO_2 (ca. 50 m^2/g) [13, 27]. On the other hand, the pore volume of mesoporous MoO_3/TiO_2 composite is 0.21 m^3/g, while the control sample is 0.17 m^3/g. Apparently, mesoporous MoO_3/TiO_2 composite has better pore structure than that of control sample.

Unlike the mesoporous MoO_3/TiO_2 composite with higher surface area and pore volume, two structural parameters of $MoO_3(I)/TiO_2$ composite are merely 37 m^2/g and 0.08 cm^3/g, respectively. It is due to that excess MoO_3 fills in the pore of TiO_2 framework, and is formed to be a composite with closed-packed structure, which is considered to have good thermal stability. In this case, the surface area of mesoporous MoO_3/TiO_2 composite is 33% lower than its precursor TiD, reflecting that the pore structure of TiO_2 framework maintains well during the preparation process. TiO_2 was obtained by calcination of TiD at 500 °C without the support. In contrast, its pore structure collapses in a certain degree compared with TiD, and the surface area of TiO_2 decreases to 103 m^2/g. Furthermore, the introduction of MoO_3 to TiO_2 also causes the shrinking of pore structure, proved by the smaller average pore size of control sample than TiO_2 (Table 1). During the whole preparation process of pathway I, the surface area loss from TiD to control sample reaches up to 60%. Obviously, the less reduction in surface area for mesoporous MoO_3/TiO_2 composite demonstrates that excess MoO_3 can effectively protect the pore structure of TiO_2 framework in preparation process as shown in pathway II of Fig. 1.

N_2 adsorption–desorption isotherms of various samples are displayed in Fig. 2. For titanate derivative, the major part of the adsorption occurs at $P/P_o < 0.4$ and no significant hysteresis appears in the isotherms. This means there are some micropores existed in the titanate derivative. Clearly, mesoporous MoO_3/TiO_2 composite shows the existence of mesopores (Fig. 2), similar to TiO_2 and control sample. This is due to the fact that the inflection of nitrogen adsorbed volume in the P/P_o range of 0.4–0.6 [28, 29], and the corresponding average pore size are shown in Table 1. Nevertheless, varying from other samples, $MoO_3(I)/TiO_2$ has the lowest quality of N_2 adsorption in the isotherm, indicating the low surface area and low porosity of $MoO_3(I)/TiO_2$. According to the literature [30], MoO_3 can be spontaneously dispersed on TiO_2 at above 450 °C even though MoO_3 was physically mixed with TiO_2 initially. Thus, it may be concluded that MoO_3 can fill in the pore of TiO_2 in $MoO_3(I)/TiO_2$ composite rather than only disperse on the external surface of TiO_2.

Figure 3 shows the XRD patterns of various samples. Strong peaks of $MoO_3(I)/TiO_2$ (Fig. 3a) at 12.8°, 23.3°, 25.7°, 27.3°, 33.7°, and 38.9° are ascribed to the diffraction patterns of (020), (110), (040), (021), (111), and (060)

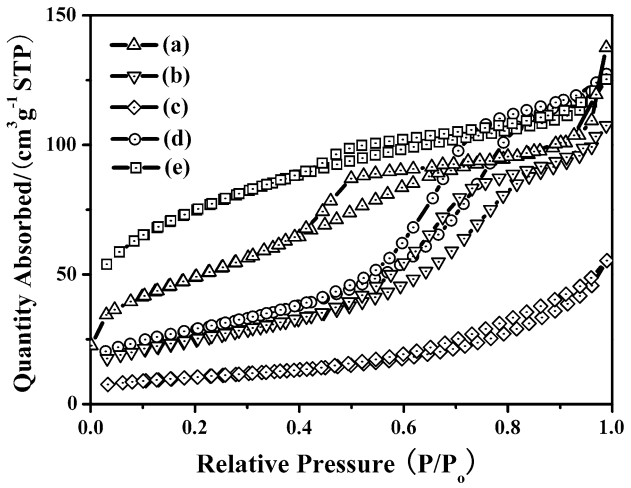

Fig. 2 N_2 adsorption–desorption isotherms of **a** MoO_3/TiO_2, **b** control sample, **c** $MoO_3(I)/TiO_2$, **d** TiO_2, **e** TiD

planes, respectively, of octahedron α-MoO_3 crystalline phase [31], while weak peaks at 25.1°, 37.8°, and 48.1° correspond to the diffraction patterns of (101), (112), and (200) planes of anatase [32]. Exactly, characteristic peaks of mesoporous MoO_3/TiO_2 composite (Fig. 3b), control sample (Fig. 3c), and TiO_2 (Fig. 3d) are in accordance with that of anatase, indicating that the crystalline phase of TiO_2 in these materials are anatase. It also suggests that the addition of MoO_3 could not influence the crystalline phase of TiO_2. As shown in Fig. 1, mesoporous MoO_3/TiO_2 composite is obtained by ammonia method from $MoO_3(I)/TiO_2$. However, there is no characteristic peaks of α-MoO_3 crystalline phase in the XRD pattern of mesoporous MoO_3/TiO_2 composite. This indicates that the excess MoO_3 can be dissolved and washed out by ammonia method, as further proved by ICP results in Table 1.

Figure 4 shows the FESEM images of mesoporous MoO_3/TiO_2 composite, control sample, and $MoO_3(I)/TiO_2$.

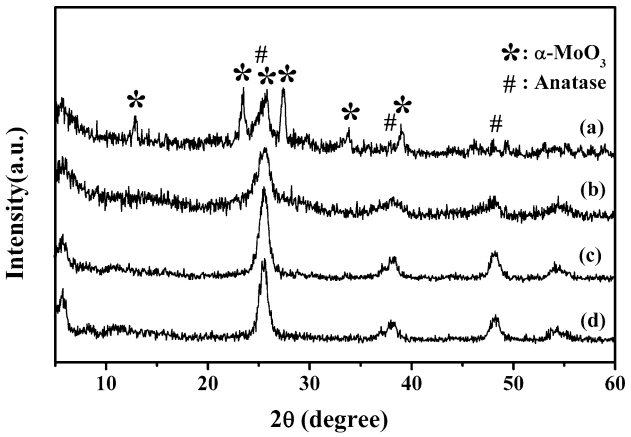

Fig. 3 XRD patterns of **a** $MoO_3(I)/TiO_2$, **b** MoO_3/TiO_2, **c** control sample, **d** TiO_2

There is no significant difference in low resolution images of all samples that consist of rods with uneven surfaces and sizes of 5–20 μm. Clearly, different from other two images, the magnified image of $MoO_3(I)/TiO_2$ (Fig. 4c) shows that the rod is packed with lots of MoO_3 nanoparticles. The agglomeration of MoO_3 nanoparticles is due to that the amount of MoO_3 is higher than the dispersion threshold. After ammonia aqueous treatment, MoO_3 nanoparticles are disappeared in the obtained mesoporous MoO_3/TiO_2 composite (seen in Fig. 4a). The surface topography of mesoporous MoO_3/TiO_2 composite is similar to that of control sample (seen in Fig. 4b). It can be seen that lots of crystal gap exist in the composite, which is corresponding to mesopores in the TiO_2 materials. It proves that MoO_3 nanoparticles can be effectively dissolved and washed away by ammonia method.

3.2 Raman Spectra

Raman spectrum technique is used to study the components on the surface of TiO_2. From Fig. 5, mesoporous MoO_3/TiO_2 composite exhibits bands at 640 and 396 cm^{-1} which are assigned to anatase phase [33]. ICP result shows that the MoO_3 content of mesoporous MoO_3/TiO_2 composite remain to be 14 wt%, but while no remarkable band corresponding to the crystal MoO_3 is observed as like in the pattern of $MoO_3(I)/TiO_2$ (Fig. 5d). This is consistent with the XRD analysis. In the magnified image at the top right corner of Fig. 4, control sample and TiO_2 are shown to identify the nature of MoO_3 species. It has been reported that the bands from 950 to 980 cm^{-1} are attributed to terminal Mo = O stretching vibrations of polymolybdate species [3]. The shoulder peak at 953 cm^{-1} is observed in MoO_3/TiO_2 composite while the relative band of control sample shifts to 964 cm^{-1}. As explained elsewhere such shifts in the Mo = O Raman frequency are related to changes in bond length and can be ascribed to an increasing interaction with the support and the deformation of three-dimensional structures [34, 35]. This means the composite with lower value of Raman shift has the better MoO_3 dispersion. Thus, this suggests the dispersion of MoO_3 in mesoporous MoO_3/TiO_2 composite is better than that in control sample.

3.3 Catalytic Tests

The results of HDS of DBT are given in Fig. 6. In contrast to control sample, MoO_3/TiO_2 composite has a higher conversion of DBT. According to the above results, the increasing conversion can be explained in terms of the relative higher MoO_3 content or better dispersion of MoO_3 in mesoporous MoO_3/TiO_2 composite. Actually, both two factors are attributed to superior pore structure of mesoporous MoO_3/TiO_2

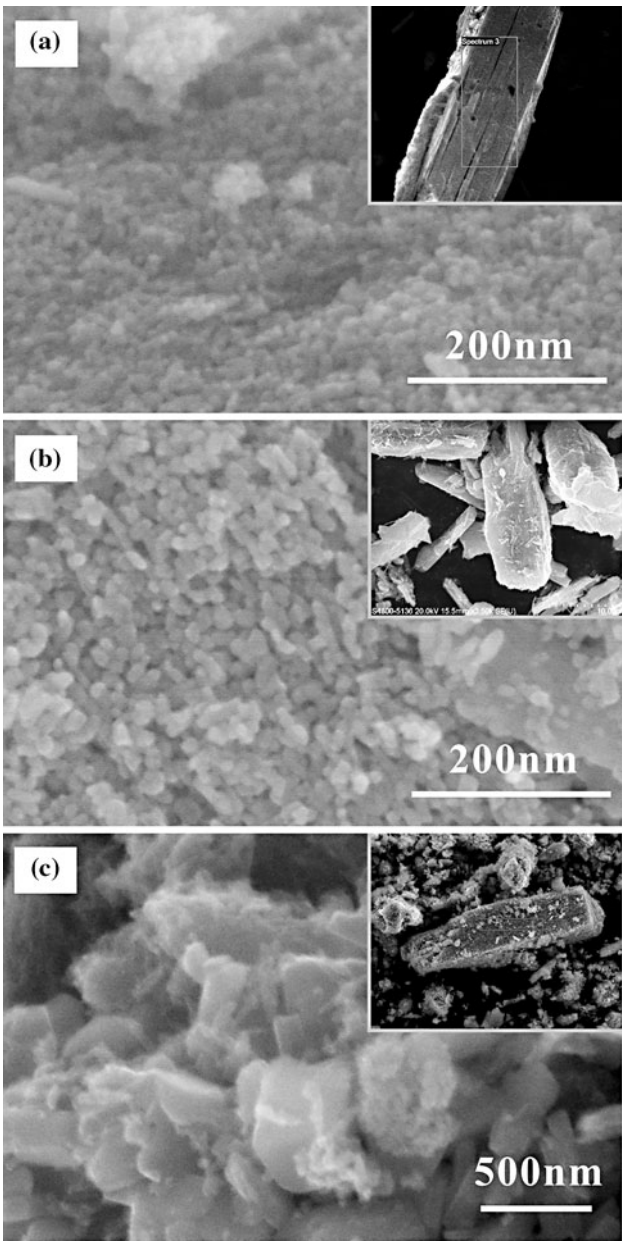

Fig. 4 FESEM images of **a** MoO_3/TiO_2, **b** control sample, **c** $MoO_3(I)/TiO_2$

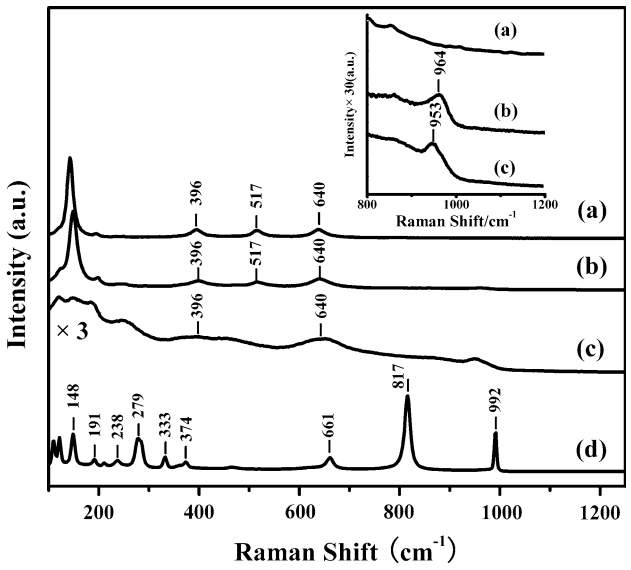

Fig. 5 Raman Spectra of **a** TiO_2, **b** control sample, **c** MoO_3/TiO_2, **d** $MoO_3(I)/TiO_2$

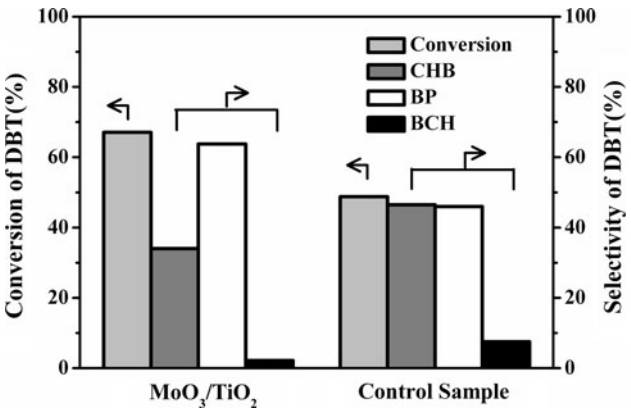

Fig. 6 HDS performances over MoO_3/TiO_2 composite and control sample

composite prepared by self-supporting and ammonia method. According to the dispersion threshold [13, 26], critical MoO_3 content of control sample (103 m^2/g, seen in Table 1) is only 12 wt% for maximum, while critical MoO_3 content can reaches up to 20 wt% or even more for mesoporous MoO_3/TiO_2 composite based on the surface area of 173 m^2/g. But in this paper, MoO_3 content of mesoporous MoO_3/TiO_2 composite attains to the critical MoO_3 content of only 70% (14 wt% of MoO_3, seen in Table 1). This suggests a good dispersion of MoO_3 in mesoporous MoO_3/TiO_2 composite.

Moreover, there is another difference in the selectivity between MoO_3/TiO_2 composite and control sample. It is well known that DBT has two HDS reaction pathways: 1) direct desulfurization (DDS), which leads to the formation of biphenyl (BP); 2) hydrogenation (HYD) yielding tetrahydrodibenzothiophene (THDBT) followed by desulfurization to cyclohexylbenzene (CHB) [36]. As is shown in Fig. 6, the mesoporous MoO_3/TiO_2 composite favors the DDS route with BP selectivity of 63.8%. And the corresponding selectivity of CHB and THDBT is 34 and 2.2%, respectively. In contrast, control sample relatively favors the HYD route (53.5%) with CHB and THDBT selectivity of 46 and 7.5%, respectively. These differences are in agreement with the results reported in the literature for DBT HDS over highly dispersed catalyst prepared via supercritical deposition or hydrothermal deposition [37, 38]. The highly dispersed catalyst has the increased proportion of the edge sites. In terms of the rim-edge model [39], it has more active sites and

simultaneously has the improved selectivity of DDS pathway of DBT HDS. Therefore, the relatively higher proportion of DDS route of HDS suggests the better MoO_3 dispersion, which is related to the superiority in the structure of mesoporous MoO_3/TiO_2 composite.

4 Conclusions

The present work described a mesoporous MoO_3/TiO_2 composite prepared from TiD by self-supporting and ammonia method. It was shown that mesoporous MoO_3/TiO_2 composite (173 m^2/g) had a higher surface area than that of control sample from mesoporous TiO_2 (90 m^2/g) by traditional impregnation. By XRD, N_2 adsorption–desorption and Raman Spectra analyses, we studied the preparation process of mesoporous MoO_3/TiO_2 composite compared with that of control sample. It could be found that the reduction in surface area of mesoporous MoO_3/TiO_2 composite from TiD was less than that of control sample due to the effect of self-supporting. The excess MoO_3 could be removed by ammonia method, and other insoluble MoO_3 species (14 wt%) still dispersed on TiO_2 were used as the catalytic active component. FESEM and Raman Spectra results showed that there are no MoO_3 particles observed in mesoporous MoO_3/TiO_2 composite, and mesoporous MoO_3/TiO_2 composite had better dispersion of MoO_3 than that of control sample. Finally, the mesoporous MoO_3/TiO_2 composite with these above characteristics were responsible for its better HDS performance.

Acknowledgments This work was supported by the Chinese National Key Technology Research and Development Program (Grant No. 2006AA03Z455), the National Basic Research Program of China (No. 2009CB226103), NSFC-RGC Joint Research Award (No. 20731160614 and HKU 735/07), Changjiang Scholars and Innovative Research Team in University (No. IRT0732), and the National Natural Science Foundation of China (Grant Nos. 20736002, 20706028, 20976080).

References

1. Coulier L, Van Veen J, Niemantsverdriet J (2002) Catal Lett 79:149
2. Ramirez J, Cede L, Busca G (1999) J Catal 184:59
3. Dzwigaj S, Louis C, Breysse A, Cattenot M, Belliere V, Geantet C, Vrinat M, Blanchard P, Payen E, Inoue S, Kudo H, Yoshimura Y (2003) Appl Catal B Environ 41:181
4. Al-Kandari H, Al-Kharafi F, Katrib A (2010) Appl Catal A Gen 383:141
5. Bourikas K, Fountzoula C, Kordulis C (2004) Appl Catal B Environ 52:145
6. Yoshitake H, Aoki Y, Hemmi S (2006) Micropor Mesopor Mater 93:294
7. Ramirez J, Macias G, Cedeno L, Gutierrez-Alejandre A, Cuevas R, Castillo P (2004) Catal Today 98:19
8. Gulkova D, Kaluza L, Vit Z, Zdrazil M (2006) Catal Lett 112:193
9. Fountzoula C, Spanos N, Matralis HK, Kordulis C (2002) Appl Catal B Environ 35:295
10. Inoue S, Muto A, Kudou H, Ono T (2004) Appl Catal A Gen 269:7
11. Boettcher SW, Fan J, Tsung CK, Shi QH, Stucky GD (2007) Acc Chem Res 40:784
12. Chen XB, Mao SS (2006) J NanoSci Nanotechnol 6:906
13. Machej T, Haber J, Turek AM, Wachs IE (1991) Appl Catal 70:115
14. Kulkarni G, Rao C (1991) Catal Lett 11:63
15. Antonelli DM, Ying JY (1995) Angew Chem Int Edit 34:2014
16. Mohammadi MR, Fray DJ, Mohammadi A (2008) Micropor Mesopor Mater 112:392
17. Jung JH, Kobayashi H, van Bommel KJC, Shinkai S, Shimizu T (2002) Chem Mater 14:1445
18. Lee DWLDW, Lee KH (2011) Micropor Mesopor Mater 142:98
19. Zhao JQ, Wan P, Xiang J, Tong T, Dong L, Gao ZN, Shen XY, Tong H (2011) Micropor Mesopor Mater 138:200
20. Zhang ZY, Zuo F, Feng PY (2010) J Mater Chem 20:2206
21. Wang H, Wu Y, Xu BQ (2005) Appl Catal B Environ 59:139
22. He M, Lu XH, Feng X, Yu L, Yang ZH (2004) Chem Comm 19:2202
23. Zhu YH, Li W, Zhou YX, Lu XH, Feng X, Yang ZH (2009) Catal Lett 127:406
24. Liu JL, Zhu YH, Yang ZH, Wang HT, Lu XH, Feng X, Wang HY (2009) Chin J Process Eng 9:882
25. Zhu YH, Zhou YX, Yang ZH, Lu XH, Feng X (2007) Acta Petrolei Sinica (Petroleum Processing Section) 23:76
26. Kim DS, Kurusu Y, Wachs IE, Hardcastle FD, Segawa K (1989) J Catal 120:325
27. Vu VH, Belkouch J, Ould-Dris A, Taouk B (2008) AIChE J 54:1585
28. Sheng QR, Yuan S, Zhang JL, Chen F (2006) Micropor Mesopor Mater 87:177
29. Kruk M, Jaroniec M (2001) Chem Mater 13:3169
30. Zi F, Guo H, Wu N, Xie Y, Hu T (2004) Chem Res Chinese U 20:685
31. Ichikuni N, Murayama H, Shimazu S, Uematsu T (2004) Catal Lett 93:177
32. Neppolian B, Celik E, Anpo M, Choi H (2008) Catal Lett 125:183
33. Zhang J, Li M, Feng Z, Chen J, Li C (2006) J Phys Chem B 110:927
34. Watson RB, Ozkan US (2002) J Catal 208:124
35. Wachs IE (1996) Catal Today 27:437
36. Nagai M, Miyao T, Tuboi T (1993) Catal Lett 18:9
37. Alibouri M, Ghoreishi SM, Aghabozorg HR (2009) AIChE J 55:2665
38. Wang H, Fan Y, Shi G, Liu ZH, Liu HY, Bao XJ (2007) Catal Today 125:149
39. Daage M, Chianelli RR (1994) J Catal 149:414